



# Unsupervised [ $^{18}\text{F}$ ]Flortaucipir cutoffs for tau positivity and staging in Alzheimer's disease

Giulia Quattrini<sup>1,2</sup> · Clarissa Ferrari<sup>3,4</sup> · Michela Pievani<sup>1</sup> · Andrea Geviti<sup>4</sup> · Federica Ribaldi<sup>5,6</sup> · Max Scheffler<sup>7</sup> · Giovanni B Frisoni<sup>5,6</sup> · Valentina Garibotto<sup>8,9,10</sup> · Moira Marizzoni<sup>1,11</sup> · for the Alzheimer's Disease Neuroimaging Initiative

Received: 1 March 2023 / Accepted: 19 May 2023 / Published online: 5 June 2023  
© The Author(s) 2023

## Abstract

**Purpose** Several [ $^{18}\text{F}$ ]Flortaucipir cutoffs have been proposed for tau PET positivity ( $T^+$ ) in Alzheimer's disease (AD), but none were data-driven. The aim of this study was to establish and validate unsupervised  $T^+$  cutoffs by applying Gaussian mixture models (GMM).

**Methods** Amyloid negative ( $A^-$ ) cognitively normal (CN) and amyloid positive ( $A^+$ ) AD-related dementia (ADRD) subjects from ADNI ( $n=269$ ) were included. ADNI ( $n=475$ ) and Geneva Memory Clinic (GMC) cohorts ( $n=98$ ) were used for validation. GMM-based cutoffs were extracted for the temporal meta-ROI, and validated against previously published cutoffs and visual rating.

**Results** GMM-based cutoffs classified less subjects as  $T^+$ , mainly in the  $A^-$  CN ( $<3.4\%$  vs  $>28.5\%$ ) and  $A^+$  CN ( $<14.5\%$  vs  $>42.9\%$ ) groups and showed higher agreement with visual rating ( $\text{ICC}=0.91$  vs  $\text{ICC}<0.62$ ) than published cutoffs.

**Conclusion** We provided reliable data-driven [ $^{18}\text{F}$ ]Flortaucipir cutoffs for in vivo  $T^+$  detection in AD. These cutoffs might be useful to select participants in clinical and research studies.

**Keywords** [ $^{18}\text{F}$ ]Flortaucipir · Alzheimer's disease · Cutoff · Gaussian mixture model · Tau PET · Tau positivity

## Introduction

Alzheimer's disease (AD) is the most common neurodegenerative disorder and is neuropathologically defined by the presence of  $\beta$ -amyloid plaques and tau neurofibrillary tangles (NFTs) [1]. NFTs are closely associated to

neurodegeneration and clinical symptoms [2, 3], and they are therefore considered an essential marker for AD diagnosis.

Tau pathology can be in vivo visualized and quantified using positron emission tomography (PET) with ligands affine to NFTs [4, 5]. Among several radioligands developed so far, [ $^{18}\text{F}$ ]Flortaucipir showed high sensitivity and specificity

✉ Moira Marizzoni  
mmarizzoni@fatebenefratelli.eu

<sup>1</sup> Laboratory of Alzheimer's Neuroimaging and Epidemiology (LANE), IRCCS Istituto Centro San Giovanni di Dio Fatebenefratelli, 25125 Brescia, Italy

<sup>2</sup> Department of Molecular and Translational Medicine, University of Brescia, 25123 Brescia, Italy

<sup>3</sup> FONDAZIONE POLIAMBULANZA ISTITUTO OSPEDALIERO via Bissolati, 57, 25124, Brescia, Italy

<sup>4</sup> Unit of Statistics, IRCCS Istituto Centro San Giovanni di Dio Fatebenefratelli, 25125 Brescia, Italy

<sup>5</sup> LANVIE – Laboratory of Neuroimaging of Aging, University Hospitals and University of Geneva, 1205 Geneva, Switzerland

<sup>6</sup> Geneva Memory Center, Department of Rehabilitation and Geriatrics, Geneva University Hospitals, 1205 Geneva, Switzerland

<sup>7</sup> Division of Radiology, Geneva University Hospitals, Geneva, Switzerland

<sup>8</sup> Laboratory of Neuroimaging and Innovative Molecular Tracers (NIMTlab), Geneva University Neurocentre, Faculty of Medicine, University of Geneva, 1205 Geneva, Switzerland

<sup>9</sup> Division of Nuclear Medicine and Molecular Imaging, University Hospitals of Geneva, 1205 Geneva, Switzerland

<sup>10</sup> Centre for Biomedical Imaging (CIBM), 1205 Geneva, Switzerland

<sup>11</sup> Biological Psychiatric Unit, IRCCS Istituto Centro San Giovanni di Dio Fatebenefratelli, 25125 Brescia, Italy

to AD-related NFTs [6, 7], and represents the first and, to date, the only tau PET tracer approved by the U.S.A. Food and Drug Administration to support the diagnosis in patients with suspected AD [8, 9]. [ $^{18}\text{F}$ ]Flortaucipir uptake correlates with histological findings of AD-related tau pathology [10–12], with phosphorylated tau (p-tau<sub>181</sub>) in the cerebral spinal fluid (CSF) [13, 14], discriminates between preclinical AD and AD-related dementia (ADRD) [11, 12], and is highly predictive of future cognitive decline and conversion of cognitively normal (CN) and mild cognitive impairment (MCI) to AD [15]. Previous studies reported that [ $^{18}\text{F}$ ]Flortaucipir regional binding topographically follows the sequential spread of NFTs [16, 17], and highlighted the strong correlation between tracer uptake, cognitive status, and disease progression [15, 17, 18]. Moreover, the presence of NFTs from stage IV onwards is consistent with a neuropathological diagnosis of AD [10, 19, 20]. This indicates that [ $^{18}\text{F}$ ]Flortaucipir PET might be extremely useful to identify AD-related pathology, to stage the disease, and to track disease progression in vivo. Along this line, AD clinical trials are starting to include [ $^{18}\text{F}$ ]Flortaucipir tau PET positivity ( $T^+$ ) status as an eligibility criterion (e.g., the TRAILBLAZER-ALZ trial investigating the donanemab antibody) [21].

Visual assessment of [ $^{18}\text{F}$ ]Flortaucipir PET scans is currently the standard method to accurately define  $T^+$  status and for staging in a clinical setting [10]. However, visual assessment of PET images requires an experienced nuclear medicine specialist, and is thus not suitable for studies that involve large numbers of subjects. This can be particularly limiting in the context of multicenter studies, which generally include hundreds or thousands of scans. Moreover, PET visual assessment is inherently subjective and may be affected by inter-rater variability. These limitations might be mitigated by using automated tools [10]. A recent study [22] reviewed thresholding methods to dichotomize [ $^{18}\text{F}$ ]Flortaucipir quantification into normal/abnormal levels, and to discriminate  $T^+$  and tau negative ( $T^-$ ) groups. Even if [ $^{18}\text{F}$ ]Flortaucipir quantifications proved to be reliable among studies [23],  $T$  status dichotomization did not. Previous approaches resulted in 82 cut-off values across 23 reviewed studies, ranging from 1.13 to 2.79. This variability is likely due to differences in (i) PET images preprocessing steps, (ii) regions-of-interest (ROIs) used to extract the cutoffs (i.e., single ROIs vs composite ROIs that included several regions involved in AD pathology and spread), (iii) clinical and demographic features of the subjects included in the analyzed cohorts, and (iv) different analytic approaches used for cut-off definition (e.g., receiver operating characteristics [ROC] curves vs a defined number of standard deviations above the mean of the reference population) [22]. Importantly, none of the previous works assessed the agreement between  $T^+$  assignment based on the proposed cutoff and PET visual rating results nor used data-driven approaches

(e.g., the Gaussian mixture models). Furthermore, the effect of factors known to impact NFTs load and propagation (e.g., presence of the allele  $\epsilon 4$  of the apolipoprotein E gene [APOE $\epsilon 4$ ], increasing age, and female sex) [18, 24–27], has never been tested.

In this study, we applied the GMM [28] on [ $^{18}\text{F}$ ]Flortaucipir quantifications to derive unsupervised cutoffs for  $T^+$  and staging. GMM-based cutoffs were internally and externally validated in two independent cohorts, and compared with published cutoffs [29–31] and visual assessment. Finally, the effect of APOE $\epsilon 4$  status, age, and sex on GMM cutoffs was tested [28].

## Material and methods

Data used in the preparation of this article were obtained from the Alzheimer's Disease Neuroimaging Initiative (ADNI) database and the Memory Center of the Geneva University Hospitals (GMC).

## Participants

### ADNI (internal validation cohort)

The ADNI (<https://adni.loni.usc.edu/>; <https://clinicaltrials.gov/ct2/show/NCT00106899>) was launched in 2003 as a public-private partnership, led by Principal Investigator Michael W. Weiner, MD [32]. The primary goal of ADNI has been to test whether serial magnetic resonance imaging (MRI), PET, other biological markers, and clinical and neuropsychological assessment can be combined to measure the progression of MCI and early AD. Each ADNI study site received approval from its institutional reviewed board. Written informed consent was obtained from all research participants. The datasets used from the ADNI database are detailed in the Appendix A of the Supplementary information. Inclusion criteria for the present study were the availability of Mini-Mental State Examination (MMSE) and Clinical Dementia Rating (CDR) scale scores, amyloid and tau PET data, as well as age, sex, and APOE genotype information. Exclusion criteria were the presence of other psychiatric disorder and a non-ADRD diagnosis at the last available visit. Subjects were classified as follows: (i) CN: MMSE $\geq 25$ , CDR=0, and consistent diagnosis throughout baseline, tau PET, and according to the last available follow-up visits; (ii) MCI: MMSE $\geq 24$ , CDR=0.5; (iii) ADRD: CDR>0.5. Subjects were then classified as amyloid negative ( $A^-$ )/positive ( $A^+$ ) according to established tracer-specific standardized uptake value ratio (SUVr) cutoffs (i.e., [ $^{18}\text{F}$ ]Florbetapir: SUVr>1.11 [33]; [ $^{18}\text{F}$ ]Florbetaben: SUVr>1.08 [34]; [ $^{18}\text{F}$ ]Flutemetamol: SUVr>0.60 [35]).

## GMC cohort (external validation)

To validate the results from ADNI in an independent and clinical cohort, we used data from the Geneva Memory Clinic (GMC) cohort. Participants were enrolled at the Centre de la Mémoire of Geneva University Hospitals (<https://www.hug.ch/centre-memoire>) from 2014 to 2022 and underwent routine clinical workup, including clinical and neuropsychological testing, and MRI. Additional procedures, such as blood collection, amyloid, tau, and fluoro-deoxyglucose (FDG) PET scans, as well as stool and saliva collection, were performed if deemed clinically useful, or in the context of other research projects [36]. MCI and ADRD stages were defined based on respective clinical diagnostic criteria [37, 38]. For the purpose of this study, GMC was considered for the external validation of GMM-based and previously published cutoffs. As for ADNI, inclusion criteria were MMSE $\geq$ 25, CDR=0 for CN, MMSE $\geq$ 24, CDR=0.5 for MCI and, CDR>0.5 for ADRD. The definition of A+ / A $^-$  was done using the same cutoffs as ADNI.

## APOE genotyping

The procedure for APOE genotyping in the ADNI cohort has been previously described [39] (Supplementary information, Appendix A).

## MRI and PET data

### Acquisition protocols

All MRI scans in both cohorts were performed on 3T scanners. MRI and PET acquisition protocols for both cohorts are reported in Appendix B of the Supplementary information. Amyloid and tau PET data were selected at the same or at the nearest available timepoint.

## Data pre-processing

### ADNI pre-processing

Pre-processing methods of 3D T1-weighted MRI and [ $^{18}$ F] Flortetapir, [ $^{18}$ F] Flortetaben, and [ $^{18}$ F] Flortetapir scan data were reported elsewhere [40]. The amyloid PET SUVR was obtained normalizing the standardized uptake value (SUV) from the mean composite cortical region (frontal, anterior

and posterior cingulate, lateral parietal, and lateral temporal cortical regions) to the conventional (non-weighted) whole cerebellum (SupplementaCite ESM.ry information, Appendix A). When amyloid and tau PET scans were performed at different timepoints, we included subjects classified as A $^+$  by the closest amyloid PET scan obtained before the tau PET scan, as no conversion to A $^-$  would have been expected at any of the future timepoints. Similarly, we included subjects classified as A $^-$  by the closest amyloid PET scan obtained after the tau PET scan. To cover the AD continuum, we included A $^-$  CN ( $n=235$ ), A $^+$  CN ( $n=117$ ), A $^+$  MCI ( $n=89$ ), and A $^+$  ADRD ( $n=34$ ). Finally, A $^-$  MCI ( $n=22$ ) were included as representative of the non-AD pathology.

### GMC pre-processing

Concerning amyloid PET, the regional amyloid SUVR from the anterior and posterior cingulate, the precuneus, and frontal, temporal, and parietal lobes was automatically quantified by the BRASS, Hermes medical solutions software (<https://www.hermesmedical.com/>). Participants were classified by applying the cutoffs mentioned above according to the used tracer.

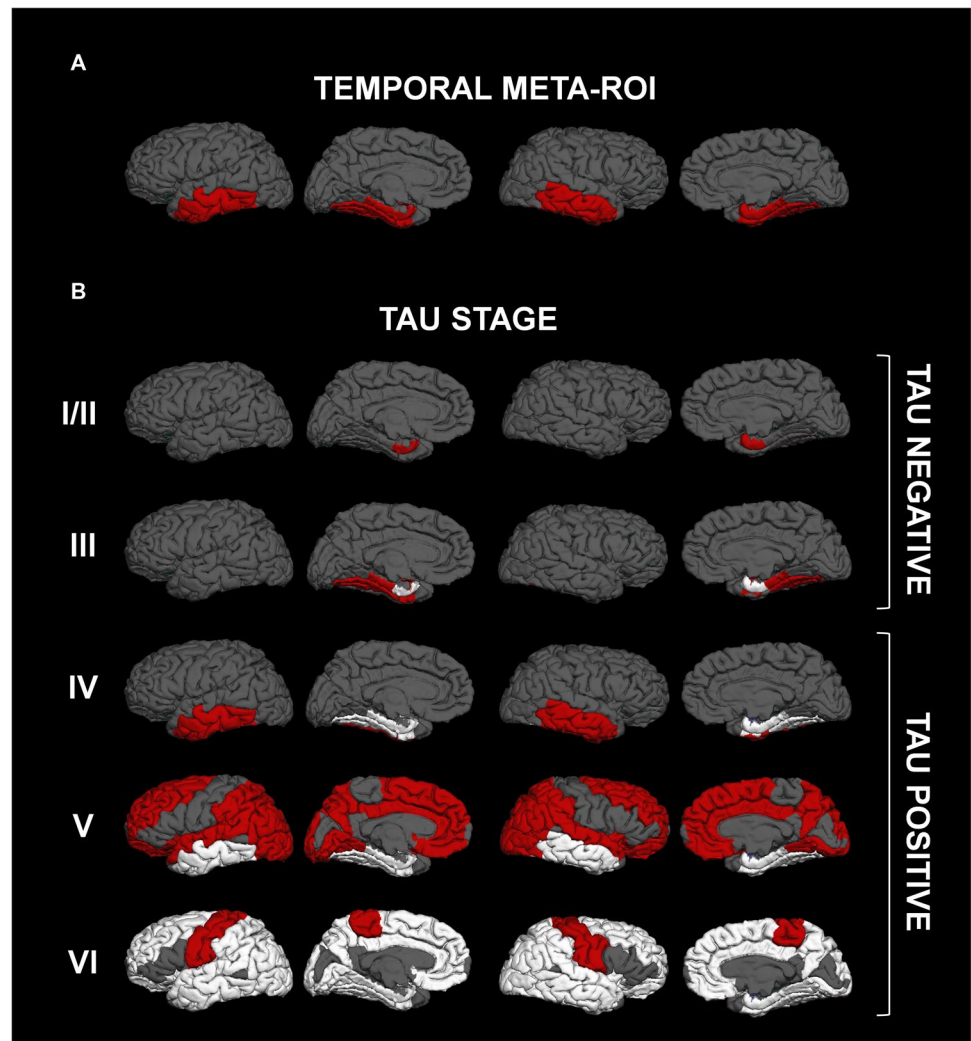
All 3D T1-weighted MRI images were visually inspected and processed using FreeSurfer v7.1 (<https://surfer.nmr.mgh.harvard.edu/>), while the [ $^{18}$ F] Flortetapir standardized uptake values (SUVs) were computed using PET-Surfer (<https://surfer.nmr.mgh.harvard.edu/fswiki/PetSurfer>) (Supplementary information, Appendix C). Finally, A $^-$  CN ( $n=29$ ), A $^+$  CN ( $n=7$ ), A $^+$  MCI ( $n=50$ ), and A $^+$  ADRD ( $n=13$ ) for the AD continuum, and A $^-$  MCI ( $n=18$ ) for the non-AD pathology were included from the GMC cohort.

### Regional [ $^{18}$ F] Flortetapir SUVR extraction

Regional [ $^{18}$ F] Flortetapir SUVR values were derived using FreeSurfer-defined regions-of-interest (ROIs). Specifically, SUVRs were derived in a temporal meta-ROI including those areas most vulnerable to NFTs-related lesions in AD [30, 41] (Fig. 1A), and in the regions corresponding to the tau spread stages (I/II, III, IV, V, and VI) as in Mattsson et al. [29] (Fig. 1B). The hippocampus (stage II) was not included, as [ $^{18}$ F] Flortetapir retention signals can be affected in this region by off-target binding of the adjacent choroid plexus [42]. To account for the varying sizes of FreeSurfer-defined ROIs, individual regional SUV weighted means (SUVR $_w$ ) were computed as follows:

$$\text{SUVR}_w = \frac{(\text{SUVR}_{\text{ROI1}} \cdot \text{VOLUME}_{\text{ROI1}}) + (\text{SUVR}_{\text{ROI2}} \cdot \text{VOLUME}_{\text{ROI2}}) + (\text{SUVR}_{\text{ROI}n} \cdot \text{VOLUME}_{\text{ROI}n})}{(\text{VOLUME}_{\text{ROI1}} + \text{VOLUME}_{\text{ROI2}} + \text{VOLUME}_{\text{ROI}n})}$$

**Fig. 1** Surface rendering of the temporal meta-ROI (A) [30] and of tau spread stages I/II–VI (B) [29] used to measure tau-PET uptake. Red regions define areas used for tau-uptake measurement. White regions indicate areas included in the previous tau-spread stage



Then, regional SUVw values were normalized to the conventional (non-weighted) inferior cerebellar gray matter (GM) intensity to obtain regional SUVr values. The highest regional SUVr value from the left and the right hemisphere was selected.

Finally, in the GMC cohort, images were visually rated as positive or negative from a board-certified specialist in nuclear medicine (VG) following published recommendations [10].

### Statistical analyses

Statistical analyses were conducted using the R software package v4.1.1 (R Foundation for statistical computing, <https://www.r-project.org/>) and the Rstudio GUI (<http://www.rstudio.com/>; version 1.3.1073). The Kruskal-Wallis test, corrected for multiple comparisons using the Dunn-Bonferroni method, was applied for continuous variable; while the Pearson chi-square test was applied for categorical variables.

For extraction of the cutoffs, the [ $^{18}\text{F}$ ]Flortaucipir SUVr of the temporal meta-ROI and individual stages of A<sup>+</sup> CN and A<sup>+</sup> ADRD from ADNI were selected. A web-based application (<http://www.admodelling.org>) [28] was used to apply the GMM on SUVr distributions to detect any underlying subgroups (mixture components), and to define the cutoff (i.e., the value for which the probability of belonging to two consecutive components is equal). To evaluate the possible effect of confounding factors on the derived cut-off, dichotomous (APOEε4: carriers/non-carriers; sex: female/male), or continuous (age: years) covariates were included in each GMM. The integrated completed likelihood criterion was computed to choose the number components of each mixture model, and thus the GMM that best fitted the data [43].

To dichotomize tau status (i.e., T<sup>-</sup> vs T<sup>+</sup>) in ADNI and GMC cohorts, we considered two approaches. In the first one, T<sup>+</sup> was defined based on GMM and previously published meta-ROI cutoffs [30, 31]. In the second one, each subject was assigned a stage based on GMM and previously

published staging cutoffs [29], and T<sup>+</sup> was defined as stages IV–VI, and T<sup>−</sup> as stages I/II–III [19, 20] (Supplementary Figure 1), according to the method routinely used in a clinical context. To assess the validity of the cutoffs in identifying tau positivity, in GMC we compared the T<sup>+</sup> percentages defined by visual assessment (rater 1), GMM-based cutoffs (rater 2) and previously published cutoffs (i.e., rater 3=Jack et al. [30], rater 4=Maass et al. [31], rater 5=Mattsson et al. [29]) using the intraclass correlation coefficient (ICC<sub>2,k</sub> between rater 1 and each other rater, and values ranging between 0 and 1, with 0 indicating no agreement among raters, and 1 indicating perfect agreement among raters).

Similarly, GMM-based tau staging was compared with that obtained with previous cutoffs and, in GMC, also with visual assessment. The stage assignment was performed as in Maass et al. [31]: first, the T<sup>+</sup> cutoff for stage VI was applied to identify subjects in stage VI; then, these subjects were removed, and the stage V cutoff was applied to identify subjects in stage V. This approach was continued until stage I/II was reached. Once also the stage I/II subjects were removed, the remaining sample was defined as T<sup>−</sup> subjects (i.e., not detected NFTs).

## Results

Table 1 summarizes subjects' features from both cohorts. In the ADNI cohort, participants underwent [<sup>18</sup>F]Florbetapir (64%) or [<sup>18</sup>F]Florbetaben (36%) amyloid PET, while in the GMC cohort participants underwent [<sup>18</sup>F]Florbetapir (46%) or [<sup>18</sup>F]Flutemetamol (54%) scans (Table 1).

### Extraction of <sup>18</sup>F-Flortaucipr SUVR GMM cutoffs

For each region, the best GMM was the one that identified two distinct components (i.e., A<sup>−</sup> CN-like and A<sup>+</sup> ADRD-like; Supplementary Table 1) and one SUVR cutoff. The resulting cutoffs were (i) for the temporal meta-ROI, 1.36; (ii) for tau stages, 1.34 (I/II), 1.35 (III), 1.38 (IV), 1.39 (V), and 1.20 (VI).

The adjustment of models for covariates did not improve the goodness of fit index, suggesting that APOE, age, and sex effects on GMMs distribution (and thus on the cut-off estimates) were negligible for cut-off extraction (Supplementary Table 2).

**Table 1** Demographic, clinical, pathological, and genetic features of participants from the Alzheimer's Disease Neuroimaging Initiative (ADNI) and the Geneva Memory Center (GMC) cohorts

Cohort	A <sup>−</sup> CN	A <sup>+</sup> CN	A <sup>−</sup> MCI	A <sup>+</sup> MCI	A <sup>+</sup> ADRD	Test value (df,3)	
						H/X <sup>2</sup>	p
ADNI, <i>n</i>	235	117	22	89	34		
Age, years	71.9±6.7	75.4±7.4	79.1±8.2 <sup>a</sup>	75.2±6.2 <sup>a</sup>	78.4±9.1 <sup>a</sup>	H=44.9	<b>&lt;.001</b>
Sex (% females)	60% <sup>c,d</sup>	59% <sup>c,d</sup>	32%	43%	56%	X <sup>2</sup> =13.0	<b>.011</b>
Education, years	17.0±2.3 <sup>e</sup>	16.8±2.3 <sup>e</sup>	17.1±2.1 <sup>e</sup>	16.3±2.5	15.2±2.1	H=21.4	<b>&lt;.001</b>
MMSE score	29.2±1.0 <sup>d,e</sup>	29.1±1.0 <sup>d,e</sup>	28.6±1.7 <sup>e</sup>	27.6±1.7 <sup>e</sup>	21.1±3.9	H=155.4	<b>&lt;.001</b>
CDR score	0.0±0.0 <sup>d,e</sup>	0.0±0.0 <sup>d,e</sup>	0.5±0.0 <sup>b</sup>	0.5±0.0 <sup>e</sup>	1.2±0.5	H=495.9	<b>&lt;.001</b>
Amyloid SUVR							
[ <sup>18</sup> F]Florbetapir	1.01±0.05	1.29±0.15 <sup>a,c</sup>	1.05±0.06	1.43±0.21 <sup>a,c</sup>	1.46±0.20 <sup>a,c</sup>	H=248.9	<b>&lt;.001</b>
[ <sup>18</sup> F]Florbetaben	1.01±0.04	1.30±0.18 <sup>a</sup>	0.99±0.0 <sup>a</sup>	1.39±0.21 <sup>a</sup>	1.63±0.19 <sup>a</sup>	H=131.8	<b>&lt;.001</b>
%APOEε4 carriers	26%	50%	9%	64%	65%	X <sup>2</sup> =61.2	<b>&lt;.001</b>
GMC, <i>n</i>	29	7	18	49	12		
Age, years	70.7±6.9	70.0±8.0	70.2±8.0	74.3±6.7	68.6±8.05	H=9.3	.055
Sex (% females)	59%	71%	38%	53%	58%	X <sup>2</sup> =2.9	.580
Education, years	16.5±4.7 <sup>e</sup>	15.3±3.6	14.1±2.9	14.0±3.4	11.3±3.9	H=11.5	<b>.022</b>
MMSE score	28.9±1.2 <sup>c,d,e</sup>	28.3±0.8 <sup>e</sup>	26.9±1.6 <sup>e</sup>	26.8±1.7	16.8±5.1 <sup>e</sup>	H=56.1	<b>&lt;.001</b>
CDR score	0.0±0.0 <sup>c,d,e</sup>	0.0±0.0 <sup>c,d,e</sup>	0.5±0.0 <sup>e</sup>	0.5±0.0 <sup>e</sup>	1.0±0.3	H=112.3	<b>&lt;.001</b>
Amyloid SUVR							
[ <sup>18</sup> F]Florbetapir	1.0±0.1 <sup>d,e</sup>	1.3±0.2	1.06±0.03 <sup>d</sup>	1.5±0.2	1.5±0.2	H=37.9	<b>&lt;.001</b>
[ <sup>18</sup> F]Flutemetamol	0.5±0.0 <sup>b,d,e</sup>	0.9±0.1 <sup>d</sup>	0.47±0.05 <sup>d,e</sup>	0.8±0.1	0.8±0.1	H=46.2	<b>&lt;.001</b>

Values are reported as mean ± standard deviation or percentage (%). H chi-square for the Kruskal-Wallis test, X<sup>2</sup> Pearson chi-square test, *p* significance level (set to < .050). of the Kruskal-Wallis test. Significance level after the Dunn-Bonferroni correction is reported for comparisons with A<sup>−</sup> CN (<sup>a</sup>), A<sup>+</sup> CN (<sup>b</sup>), A<sup>−</sup> MCI (<sup>c</sup>), A<sup>+</sup> MCI (<sup>d</sup>), A<sup>+</sup> ADRD (<sup>e</sup>), and significant results are reported in bold. MMSE Mini-Mental State Examination Test, CDR Clinical Dementia Rating Scale, APOEε4 Apolipoprotein E ε4 allele, A<sup>−</sup> amyloid negative, A<sup>+</sup> amyloid positive, CN cognitively normal, MCI mild cognitive impairment, ADRD Alzheimer's disease-related dementia, *n* number, *df* degrees of freedom, SUVR standardized uptake value ratio



## T<sup>+</sup> classification

In ADNI, the percentage of subjects classified as T<sup>+</sup> using the GMM cutoff for the temporal meta-ROI were 2% and 13% for A<sup>-</sup> and A<sup>+</sup> CNs, respectively, 49% for A<sup>+</sup> MCI, 85% for A<sup>+</sup> ADRD, and 18% of A<sup>-</sup> MCI (Fig. 2A, solid orange line). Similar percentages were found for GMC study participants, where subjects were labeled as T<sup>+</sup> in 3% and 14% of A<sup>-</sup> and A<sup>+</sup> CNs respectively, 55% of A<sup>+</sup> MCI, 67% of A<sup>+</sup> ADRD, and 11% of A<sup>-</sup> MCI cases (Fig. 2B, solid orange line). These proportions were confirmed when tau status was calculated based on stages' dichotomization for both cohorts (Fig. 2, dashed red line). Frequencies of T<sup>+</sup> according to the previously published thresholds for the temporal meta-ROI (i.e., Jack et al.: SUVR>1.19 [30]; Maass et al.: SUVR>1.20 [31]), and to the dichotomization of stages (i.e., from stage I-II to stage VI: 1.28, 1.23, 1.31, 1.16, 1.09, according to Mattsson et al. [29], were higher in both cohorts (Fig. 2). Finally, the T<sup>+</sup> classification using the visual assessment, considered as the clinical standard for T<sup>+</sup> identification, was 0% and 14% for A<sup>-</sup> and A<sup>+</sup> CNs, respectively, 69% for A<sup>+</sup> MCI, 75% for A<sup>+</sup> ADRD, and 6% of A<sup>-</sup> MCI (Fig. 2B). Concordance with the visual assessment was higher for GMM cutoffs (ICC=0.91 for temporal meta-ROI and ICC=0.86 for stages' dichotomization) than for previous cutoffs (ICC=0.65 [30], and ICC=0.67 [31] for temporal meta-ROI and ICC=0.64 [29] for stages' dichotomization) (Fig. 2B).

## Tau staging

In ADNI, GMM cutoffs for tau staging showed for subjects classified as free from detectable NFTs a percentage of 96% of A<sup>-</sup> CN, 76% of A<sup>+</sup> CNs, 35% of A<sup>+</sup> MCI, and 64% of A<sup>-</sup> MCI (Fig. 3A). Among A<sup>+</sup> MCI, 20% were at stage V,

and 19% at stage IV, while A<sup>+</sup> ADRD were mainly classified as stages VI (38%) and V (29%) (Fig. 3B). According to previously published cutoffs for staging [29], 68% of A<sup>-</sup> CN, 55% of A<sup>+</sup> CN, and 13% of A<sup>+</sup> MCI were classified as free from detectable NFTs (Fig. 3A). The majority of A<sup>+</sup> MCI patients were classified as stages IV, III, and VI (36%, 23%, 19%), A<sup>+</sup>ADRD patients as stage IV and VI (65%, 15%), and A<sup>-</sup> MCI as stage V (77%) and VI (23%) (Fig. 3B). The analysis in the GMC cohort confirmed the higher frequency of free from detectable NFTs subjects in the CN and A<sup>+</sup> MCI groups for GMM cutoffs (A<sup>-</sup> CN, 79%; A<sup>+</sup> CN, 71%, A<sup>+</sup> MCI, 24%), compared to Mattsson et al. cutoffs (A<sup>-</sup> CN, 45%; A<sup>+</sup> CN, 43%; A<sup>+</sup> MCI, 10%) (Fig. 3C), while a lower percentage was reported for A<sup>-</sup> MCI (i.e., 78% and 61%, for GMM and Mattsson cutoffs, respectively). As in ADNI, Mattsson cutoffs found higher frequencies of T<sup>+</sup> subjects in stages V (from A<sup>-</sup> CN to ADRD: 14%, 29%, 43%, 50%) and VI (from A<sup>-</sup> CN to ADRD: 34%, 29%, 33%, 33%), compared to GMM-based ones (Fig. 3D).

Concordance with the clinical standard (visual assessment) was higher for GMM cutoffs (ICC=0.83) than for Mattsson's cutoffs [29] (ICC=0.59) (Fig. 3D).

## Discussion

The in vivo detection of pathological NFT deposition is of primary importance for AD diagnosis and monitoring [1–3]. Here, we developed data-driven [<sup>18</sup>F]Flortaucipir SUVR cutoffs for the in vivo assignment of tau positivity and tau staging, and validated them in two independent cohorts. Furthermore, we compared the derived cutoffs with previously published thresholds and visual assessment.

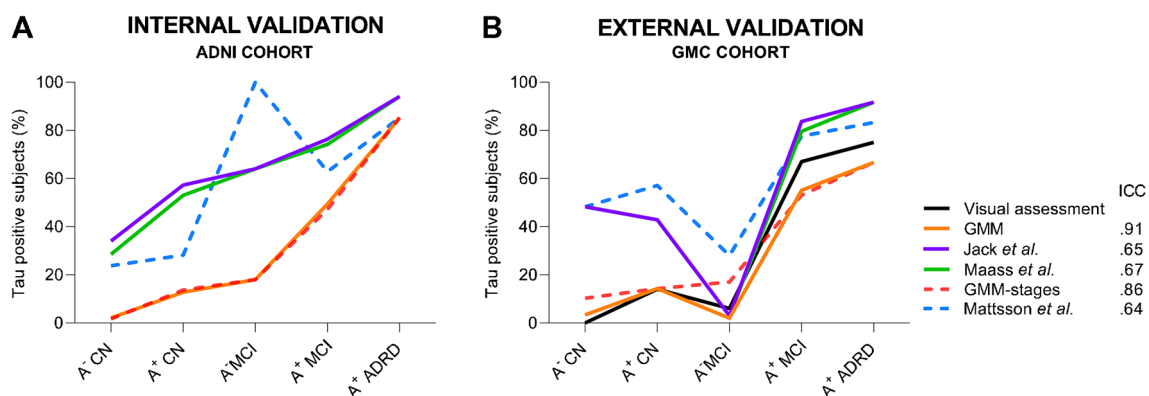


**Fig. 2** Percentage of subjects classified as tau positive (T<sup>+</sup>) based on different temporal meta-ROI cutoffs, and by grouping stage-based cutoffs (dashed lines). The performance of the GMM and previously published cutoffs was tested in ADNI (internal validation, **A**) and validated in

GMC (external validation, **B**). Concordance with the clinical standard (i.e., visual assessment), was tested in the GMC cohort with the intra-class correlation coefficients (ICCs). The Gaussian mixture models (GMM) cutoffs showed the highest agreement with the clinical standard

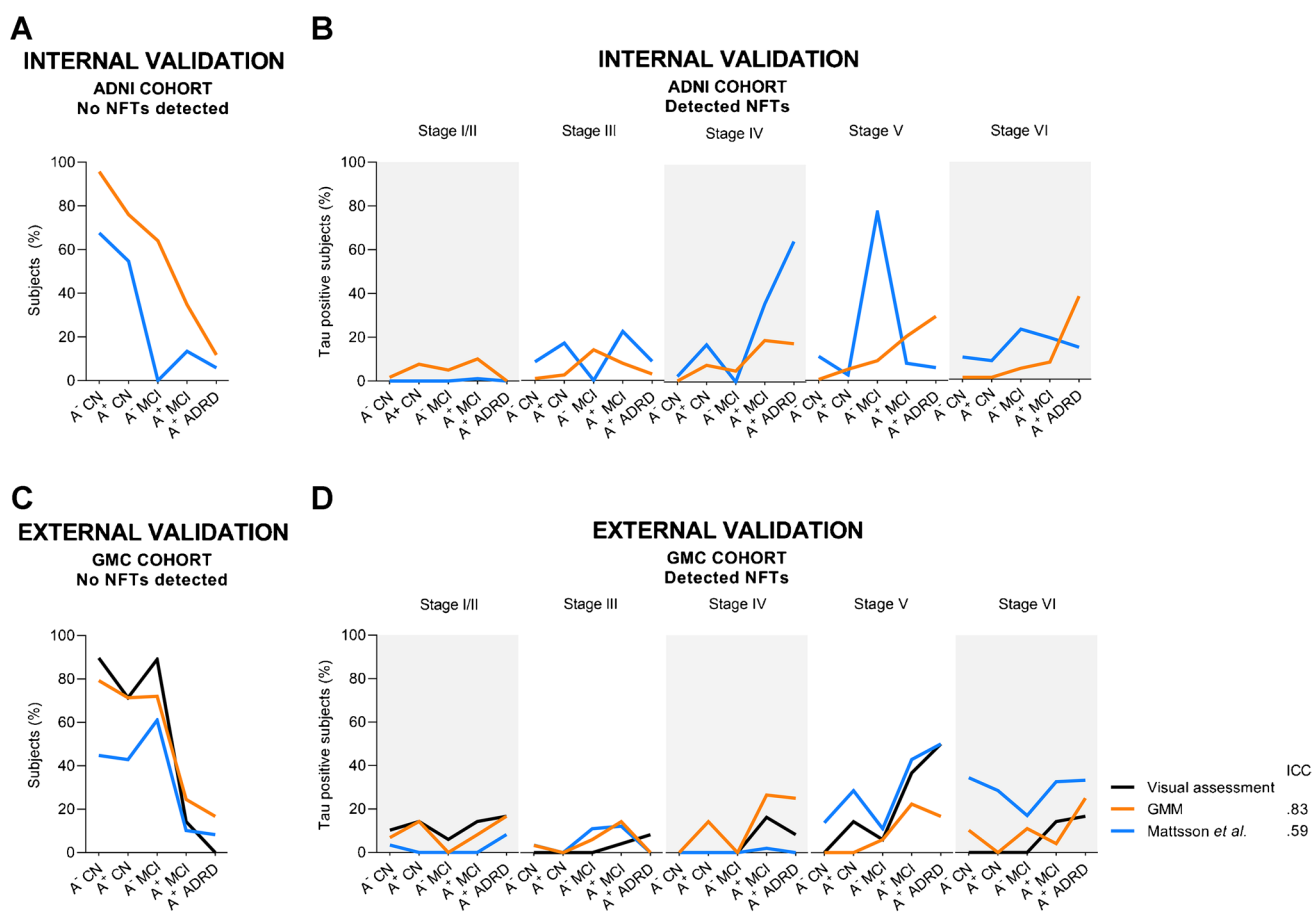


**Fig. 3** Percentage of subjects classified as tau positive ( $T^+$ ) based on the different tau stages' cutoffs. The performance of the cutoffs was tested in ADNI (internal validation, panels **A**, **B**) and GMC (external validation, panels **C**, **D**). Concordance with the clinical

standard (i.e., visual assessment) was tested in the GMC cohort with intra-class correlation coefficients (ICCs; **D**). The Gaussian mixture models (GMM) cutoffs showed the highest agreement with the clinical standard

Results from ADNI and GMC were consistent with each other and with previous [ $^{18}\text{F}$ ]Flortaucipir PET studies showing that  $A^-$  CN subjects are usually free of tau pathology, that  $A^+$  CN might have NFTs deposition beyond the medial temporal region (i.e., from stage IV onwards) [44–47], that half of  $A^+$  MCI patients were in stage III or lower, and that the majority of  $A^+$  ADRD were classified from stage III or higher [16, 19, 48]. For  $A^-$  MCI, frequencies found applying GMM-based cutoffs were similar to those reported by Altomare et al. (11%) in the same cohort [49]. Percentages of  $T^+$  assigned subjects using GMM-based cutoff for the temporal meta-ROI were also similar to those reported in a previous multi-cohort study applying a similar [ $^{18}\text{F}$ ]Flortaucipir threshold (i.e.,  $\text{SUVR}=1.34$ ) [46]. Furthermore, the  $T^+$  and stage assignments according to GMM-based cutoffs were highly consistent with visual assessment and outperformed other cutoffs, revealing an excellent agreement ( $\text{ICC} \geq 0.85$ ) [50]. The large proportion of  $A^+$  MCI in stage III or lower (up to 53%) could be explained by the low reliability of [ $^{18}\text{F}$ ]Flortaucipir to detect NFTs in the early Braak

stages [16, 42, 51], but it might also suggest that these subjects were at a very early stage of the disease or represented the Alzheimer's and concomitant suspected non-Alzheimer's pathologic change category [ $A^+T^-$  ( $N^+$ )] [1]. To test this possibility, we retrospectively reviewed CSF total tau and p-tau<sub>181</sub> levels in the ADNI cohort [29, 52, 53]. CSF total tau is a marker of neurodegeneration ( $N^+$ ) [1], and p-tau<sub>181</sub> is sensitive to tau pathology possibly earlier than tau PET [29, 52, 53]. Among the  $A^+T^-$  MCI patients classified as stage III or lower using PET, 25 out of 46 had CSF data. Of these, 56% were identified as borderline (20.59–27.41 pg/ml) or  $T^+$  according to the p-tau<sub>181</sub> cutoff (27.41 pg/ml) [54] and 100% as  $N^+$  according to the total-tau CSF cutoff (104.15 pg/ml) [54]. These results confirmed that  $A^+/(CSF) T^+$  (PET) $T^-$  subjects were likely in an early disease stage, while  $A^+/(CSF \text{ and PET}) T^-$  subjects might represent the  $A^+TN^+$  category [1]. GMM cutoffs also identified up to 10% of  $A^-$  CN subjects (GMC cohort) in stage IV or higher. This might be indicative of false positives or, alternatively, other diseases than AD (e.g., suspected non-AD pathophysiology

[SNAP; i.e.,  $A^{-}T^{+}(N)^{-}$ ,  $A^{-}T^{-}(N)^{+}$  or  $A^{-}T^{+}(N)^{+}$ ] [55] or primary age-related tauopathy [PART]) [56]. Again, we retrospectively reviewed CSF total tau and p-tau<sub>181</sub> levels in the ADNI cohort. Data were available for 3 out of 4  $A^{-}$  CN classified as stage IV or higher. For them, the detected patterns were  $A^{-}T^{-}(N)^{+}$  (1 subject) or  $A^{-}T^{+}(N)^{+}$  (2 subjects), thus confirming that they might represent the SNAP category.

The GMM cutoff for the temporal meta-ROI is consistent with that identified by a recent study [41] assessing the optimal ROI and [ $^{18}\text{F}$ ]Flortaucipir SUVR threshold for the differential diagnosis of ADRD vs CN and other neurodegenerative conditions. Apart from this recent study, GMM values were generally higher than previously published cutoffs [29–31] and identified a lower number of  $T^{+}$  subjects, regardless of diagnostic groups and cohorts, possibly indicating that GMM thresholds are more conservative. This is likely related to the different methods applied for cut-off extraction. To the best of our knowledge, this is the first study that applied a data-driven approach to identify [ $^{18}\text{F}$ ]Flortaucipir SUVR values for  $T^{+}$  and staging. Previous works used the 95% percentile (i.e., mean plus two standard deviations) based on young [30] or older [29] CN subjects as well as the ROC with Youden index between  $A^{-}$  CN and  $A^{+}$  MCI and AD [31]. The higher percentages of  $T^{+}$  within the  $A^{-}$  CN found with the previously published cutoffs [29–31] suggest that the latter group might be more susceptible to false positives than GMM cutoffs. This explanation is supported by the higher agreement of GMM cutoffs with the clinical standard ( $\text{ICC} > 0.85$ ), as compared with other cutoffs ( $\text{ICC} < 0.62$ ).

In this work, we assessed the effect of the main risk factors for AD (APOE $\epsilon$ 4 status, increasing age, female sex) on cut-off extraction. Contrary to what was expected, none of these variables affected the cut-off estimations [18, 24, 46]. The lack of effect of risk factors on tau PET positivity cutoffs might be related to a priori selection criteria in the derivation sample. Indeed, while  $A^{-}$  CN were mainly younger non-carrier females,  $A^{+}$  ADRD dementia cases were generally older carrier males, thus possibly accounting for most of the APOE $\epsilon$ 4, age, and sex confounding effects. Alternatively, the limited size of the  $A^{+}$  ADRD group may have prevented our group from observing any significant effect on cutoffs' derivation.

The main strength of this work was the application of a probabilistic data-driven approach to derive unbiased cutoffs for [ $^{18}\text{F}$ ]Flortaucipir positivity definition. The strength of unsupervised methods lies in their independence from sample features (e.g., diagnostic information), meaning they are not affected by any related potential bias. Secondly, the derived cutoffs were validated in an independent cohort from a memory clinic population, thus supporting generalizability to clinical settings. Finally, the results were validated against visual rating, which is the standard for tau PET assessment

in clinical practice. The high agreement between visual rating and GMM cutoffs suggests that these unbiased cutoffs may be a helpful complement to support visual rating in a clinical context. These cutoffs could help physicians in diagnosis by increasing diagnostic confidence [49]. In addition, once anti-amyloid and anti-tau drugs become commercially available, the cutoffs could be used for targeted enrollment of participants according to tau stage. On the other hand, in a research context, they might provide a useful measure of disease stage or progression, which may be useful for both study participant classification and outcome assessment. Finally, as GMM-based cutoffs classified a lower number of  $T^{+}$  subjects in the CN group compared to previously published thresholds, they might reduce misdiagnoses and inclusion of non-AD pathologies in future clinical trials. The main limitation of the present study is the small sample size of some subgroups (e.g.,  $A^{+}$  CN,  $A^{-}$  MCI, and  $A^{+}$  ADRD), and lacking representation of  $A^{-}$  ADRD group. Future studies including larger sample size of these groups, and also considering well-characterized non-AD neurodegenerative diseases, are needed to confirm the GMM cut-off performance. Secondly, the lack of autopsy data prevents the validation of the cutoffs against histologically confirmed amyloid and tau pathology. Indeed, a high but not complete concordance between PET and histology was reported both for amyloid and tau pathology [10, 51, 57, 58], and we cannot exclude that did not have an impact on our results. Also, the possibility of misdiagnoses should be accounted for in both cohorts. Another limiting factor is the lack of follow-up data, which would have offered valuable clinical feedback on the potential usefulness of our cutoffs in terms of disease monitoring and progression tracking. Lastly, despite the fact that [ $^{18}\text{F}$ ]Flortaucipir has been approved for staging in AD, we must acknowledge its limited reliability in detecting NFTs in early disease stages.

## Conclusion

The mixture modeling approach enabled the identification of reliable and unbiased [ $^{18}\text{F}$ ]Flortaucipir cutoffs for tau positivity and staging supporting their use in both research and clinical settings.

**Supplementary information** The online version contains supplementary material available at <https://doi.org/10.1007/s00259-023-06280-7>.

**Acknowledgements** The authors wish to thank the Alzheimer's Disease Neuroimaging Initiative (ADNI) for providing data for these analyses. Data used in preparation of this article were obtained from the ADNI database ([adni.loni.usc.edu](http://adni.loni.usc.edu)). As such, the investigators within the ADNI contributed to the design and implementation of ADNI and/or provided data but did not participate in analysis or writing of this report. A complete listing of ADNI investigators can be found at: [http://adni.loni.usc.edu/wp-content/uploads/how\\_to\\_apply/](http://adni.loni.usc.edu/wp-content/uploads/how_to_apply/)



[ADNI\\_Acknowledgement\\_List.pdf](#). Avid radiopharmaceuticals provided access to the [ $^{18}\text{F}$ ]Flortaucipir radiotracer for the GMC cohort but was not involved in data analysis or interpretation. The Clinical Research Center, at Geneva University Hospital and Faculty of Medicine provides valuable support for regulatory submissions and data management, and the Biobank at Geneva University Hospital for biofluid processing and storage.

**Author contribution** Conceptualization: GQ, MM; methodology: GQ, CF, MP, AG, MM; formal analysis: GQ; data curation: GQ, FR, MS, VG; writing - original draft: GQ, CF, MP, MM; writing - review & editing: GQ, CF, MP, AG, FR, MS, GBF, VG, MM; supervision: MP, GBF, VG, MM; funding acquisition: MM; supervision, writing - original draft, writing - review & editing.

**Funding** The research leading to the present results has received funding from the Alzheimer's Association under grant agreement n° GEENA-Q-19-595850 (The dark side of APOE  $\epsilon$ 4: unraveling amyloid-independent effects in AD), and was partially supported by grants from Italian Ministry of Health (Ricerca Corrente). The Centre de la mémoire is funded by the following private donors under the supervision of the Private Foundation of Geneva University Hospitals: A.P.R.A. - Association Suisse pour la Recherche sur la Maladie d'Alzheimer, Genève; Fondation Segré, Genève; Race Against Dementia Foundation, London, UK; Fondation Child Care, Genève; Fondation Edmond J. Safra, Genève; Fondation Minkoff, Genève; Fondazione Agusta, Lugano; McCall Macbain Foundation, Canada; Nicole et René Keller, Genève; Fondation AETAS, Genève. Competitive research projects have been funded by: H2020 (projects n. 667375), Innovative Medicines Initiative (IMI contract n. 115736 and 115952), IMI2, Swiss National Science Foundation (projects n.320030\_182772 and n.320030\_169876), VELUX Foundation. VG was funded by the Swiss National Science Foundation (projects 320030\_185028, IZSEZO\_188355 and 320030\_169876), Aetas foundation, Velux foundation and Schmidheiny foundation.

**Data availability** All data and materials support their published claims and comply with field standards. The datasets generated during the current study are available in the ADNI repository ([adni.loni.usc.edu/](http://adni.loni.usc.edu/)), and on request for the GMC cohort.

## Declarations

**Ethics approval** Each study site and the received approval from its institutional reviewed board. This human study is compliant with the Code of Ethics of the World Medical Association (Declaration of Helsinki).

**Consent to participate** All research participants provided written informed consent.

**Competing interests** The authors declare no competing interests.

**Open Access** This article is licensed under a Creative Commons Attribution 4.0 International License, which permits use, sharing, adaptation, distribution and reproduction in any medium or format, as long as you give appropriate credit to the original author(s) and the source, provide a link to the Creative Commons licence, and indicate if changes were made. The images or other third party material in this article are included in the article's Creative Commons licence, unless indicated otherwise in a credit line to the material. If material is not included in the article's Creative Commons licence and your intended use is not permitted by statutory regulation or exceeds the permitted use, you will need to obtain permission directly from the copyright holder. To view a copy of this licence, visit <http://creativecommons.org/licenses/by/4.0/>.

## References

1. Jack CR Jr, Bennett DA, Blennow K, Carrillo MC, Dunn B, Haeberlein SB, Holtzman DM, Jagust W, Jessen F, Karlawish J, NIA-AA Research framework: toward a biological definition of Alzheimer's disease. *Alzheimer's Dement.* 2018;14:535–62.
2. Bejanin A, Schonhaut DR, La Joie R, Kramer JH, Baker SL, Sosa N, Ayakta N, Cantwell A, Janabi M, Lauriola M. Tau pathology and neurodegeneration contribute to cognitive impairment in Alzheimer's disease. *Brain.* 2017;140:3286–300.
3. Hanseeuw BJ, Betensky RA, Jacobs HI, Schultz AP, Sepulcre J, Becker JA, Cosio DMO, Farrell M, Quiroz YT, Mormino EC. Association of amyloid and tau with cognition in preclinical Alzheimer disease: a longitudinal study. *JAMA Neurol.* 2019;76:915–24.
4. Betthausen TJ. AD molecular: Imaging tau aggregates with positron emissions tomography. *Progress Mol Biol Transl Sci.* 2019;165:107–38.
5. Wang YT, Edison P. Tau imaging in neurodegenerative diseases using positron emission tomography. *Curr Neurol Neurosci Rep.* 2019;19:1–14.
6. Wolters E, Dodich A, Boccardi M, Corre J, Drzezga A, Hansson O, Nordberg A, Frisoni G, Garibotto V, Ossenkoppele R. Clinical validity of increased cortical uptake of [ $^{18}\text{F}$ ] flortaucipir on PET as a biomarker for Alzheimer's disease in the context of a structured 5-phase biomarker development framework. *Eur J Nucl Med Mol Imaging.* 2021;48:2097–109.
7. Zhang W, Xu S, Yu H, Li X, Jin Z, Li Y, He Z. Radioactive synthesis of tau PET imaging agent 18F-AV-1451 and its role in monitoring the progression of Alzheimer's disease and supporting differential diagnosis. *Ann Nucl Med.* 2021;35:139–47.
8. Jie CV, Treyer V, Schibli R, Mu L. Tauvid™: The first FDA-approved PET tracer for imaging tau pathology in Alzheimer's disease. *Pharmaceuticals (Basel).* 2021;14:110.
9. US Food and Drug Administration. FDA approves first drug to image tau pathology in patients being evaluated for Alzheimer's disease. Silver Spring, MD: Food and Drug Administration; 2020.
10. Fleisher AS, Pontecorvo MJ, Devous MD, Lu M, Arora AK, Trucchio SP, Aldea P, Flitter M, Locascio T, Devine M. Positron emission tomography imaging with [ $^{18}\text{F}$ ] flortaucipir and postmortem assessment of Alzheimer disease neuropathologic changes. *JAMA Neurol.* 2020;77:829–39.
11. Gordon BA, Friedrichsen K, Brier M, Blazey T, Su Y, Christensen J, Aldea P, McConathy J, Holtzman DM, Cairns NJ. The relationship between cerebrospinal fluid markers of Alzheimer pathology and positron emission tomography tau imaging. *Brain.* 2016;139:2249–60.
12. Mattsson N, Smith R, Strandberg O, Palmqvist S, Schöll M, Insel PS, Hägerström D, Ohlsson T, Zetterberg H, Blennow K. Comparing 18F-AV-1451 with CSF t-tau and p-tau for diagnosis of Alzheimer disease. *Neurol.* 2018;90:e388–95.
13. La Joie R, Bejanin A, Fagan AM, Ayakta N, Baker SL, Bourakova V, Boxer AL, Cha J, Karydas A, Jerome G, Maass A, Mensing A, Miller ZA, O'Neil JP, Pham J, Rosen HJ, Tsai R, Visani AV, Miller BL, et al. Associations between [ $^{18}\text{F}$ ]AV1451 tau PET and CSF measures of tau pathology in a clinical sample. *Neurol.* 2018;90:e282–90.
14. Meyer P, Binette AP, Gonneaud J, Breitner JC, Villeneuve S, Investigators ADNI. Characterization of Alzheimer disease biomarker discrepancies using cerebrospinal fluid phosphorylated tau and AV1451 positron emission tomography. *JAMA Neurol.* 2020;77:508–16.
15. Biel D, Brendel M, Rubinski A, Buerger K, Janowitz D, Dichgans M, Franzmeier N. Tau-PET and in vivo Braak-staging

- as prognostic markers of future cognitive decline in cognitively normal to demented individuals. *Alzheimer's Res Ther*. 2021;13:1–13.
16. Schwarz AJ, Yu P, Miller BB, Shcherbinin S, Dickson J, Navitsky M, Joshi AD, Devous MD Sr, Mintun MS. Regional profiles of the candidate tau PET ligand 18 F-AV-1451 recapitulate key features of Braak histopathological stages. *Brain*. 2016;139:1539–50.
  17. Cho H, Lee HS, Choi JY, Lee JH, Ryu YH, Lee MS, Lyoo CH. Predicted sequence of cortical tau and amyloid- $\beta$  deposition in Alzheimer disease spectrum. *Neurobiol Aging*. 2018;68:76–84.
  18. Pontecorvo MJ, Devous MD Sr, Navitsky M, Lu M, Salloway S, Schaerf FW, Jennings D, Arora AK, McGeehan A, Lim NC. Relationships between flortaucipir PET tau binding and amyloid burden, clinical diagnosis, age and cognition. *Brain*. 2017;140:748–63.
  19. Lowe VJ, Lundt ES, Albertson SM, Min H, Fang P, Przybelski SA, Senjem ML, Schwarz CG, Kantarci K, Boeve B. Tau-positron emission tomography correlates with neuropathology findings. *Alzheimers Dement*. 2020;16:561–71.
  20. Sonni I, Lesman Segev OH, Baker SL, Iaccarino L, Korman D, Rabinovici GD, Jagust WJ, Landau SM, La Joie R. Alzheimer's Disease neuroimaging initiative. evaluation of a visual interpretation method for tau-PET with 18F-flortaucipir. *Alzheimer's Dement Diagn Assess Dis Monit*. 2020;12:e12133.
  21. Mintun MA, Lo AC, Duggan Evans C, Wessels AM, Ardayio PA, Andersen SW, Shcherbinin S, Sparks J, Sims JR, Brys M. Donanemab in early Alzheimer's disease. *N Engl J Med*. 2021;384:1691–704.
  22. Weigand AJ, Maass A, Eglit GL, Bondi MW. What's the cut-point?: a systematic investigation of tau PET thresholding methods. *Alzheimer's Res Ther*. 2022;14:1–17.
  23. Devous MDS, Joshi AD, Navitsky M, Southekal S, Pontecorvo MJ, Shen H, Lu M, Shankle WR, Seibyl JP, Marek K, Mintun MA. Test-retest reproducibility for the tau PET Imaging agent flortaucipir F 18. *J Nucl Med*. 2018;59:937–43.
  24. La Joie R, Visani AV, Lesman-Segev OH, Baker SL, Edwards L, Iaccarino L, Soleimani-Meigooni DN, Mellinger T, Janabi M, Miller ZA, Perry DC, Pham J, Strom A, Gorno-Tempini ML, Rosen HJ, Zaller BL, Jagust WJ, Rabinovici GD. Association of APOE4 and clinical variability in Alzheimer Disease with the pattern of tau- and amyloid-PET. *Neurol*. 2021;96:e650–61.
  25. Theriault J, Benedet AL, Pascoal TA, Mathotaarachchi S, Chamous M, Savard M, Thomas E, Kang MS, Lussier F, Tissot C. Association of apolipoprotein E  $\epsilon$ 4 with medial temporal tau independent of amyloid- $\beta$ . *JAMA Neurol*. 2020;77:470–9.
  26. Shokouhi S, Taylor WD, Albert K, Kang H, Newhouse PA. Alzheimer's Disease Neuroimaging Initiative. In vivo network models identify sex differences in the spread of tau pathology across the brain. *Alzheimer's Dement Diagn Assess Dis Monit*. 2020;12:e12016.
  27. Buckley RF, Mormino EC, Rabin JS, Hohman TJ, Landau S, Hansseuw BJ, Jacobs HI, Papp KV, Amariglio RE, Properzi MJ. Sex differences in the association of global amyloid and regional tau deposition measured by positron emission tomography in clinically normal older adults. *JAMA Neurol*. 2019;76:542–51.
  28. Marizzoni M, Ferrari C, Babiloni C, Albani D, Barkhof F, Cavaliere L, Didic M, Forloni G, Fusco F, Galluzzi S. CSF cutoffs for MCI due to AD depend on APOE $\epsilon$ 4 carrier status. *Neurobiol Aging*. 2020;89:55–62.
  29. Mattsson N, Schöll M, Strandberg O, Smith R, Palmqvist S, Insel PS, Hägerström D, Ohlsson T, Zetterberg H, Jögi J. 18F-AV-1451 and CSF T-tau and P-tau as biomarkers in Alzheimer's disease. *EMBO Mol Med*. 2017;9:1212–23.
  30. Jack CR Jr, Wiste HJ, Weigand SD, Therneau TM, Lowe VJ, Knopman DS, Gunter JL, Senjem ML, Jones DT, Kantarci K. Defining imaging biomarker cut points for brain aging and Alzheimer's disease. *Alzheimer's Dement*. 2017;13:205–16.
  31. Maass A, Landau S, Baker SL, Horng A, Lockhart SN, La Joie R, Rabinovici GD, Jagust WJ. Alzheimer's Disease neuroimaging initiative. Comparison of multiple tau-PET measures as biomarkers in aging and Alzheimer's disease. *Neuroimage*. 2017;157:448–63.
  32. Petersen RC, Aisen PS, Beckett LA, Donohue MC, Gamst AC, Harvey DJ, Jack CR Jr, Jagust WJ, Shaw LM, Toga AW, Trojanowski JQ, Weiner MW. Alzheimer's disease neuroimaging initiative (ADNI): clinical characterization. *Neurol*. 2010;74:201–9.
  33. Joshi AD, Pontecorvo MJ, Clark CM, Carpenter AP, Jennings DL, Sadowsky CH, Adler LP, Kovnat KD, Seibyl JP, Arora A, Saha K, Burns JD, Lowrey MJ, Mintun MA, Skovronsky DM, Flortetapir F, 18 Study Investigators. Performance characteristics of amyloid PET with flortetapir F 18 in patients with Alzheimer's disease and cognitively normal subjects. *J Nucl Med*. 2012;53:378–84.
  34. Royse SK, Minhas DS, Lopresti BJ, Murphy A, Ward T, Koeppe RA, Bullich S, DeSanti S, Jagust WJ, Landau SM. Validation of amyloid PET positivity thresholds in centiloids: a multisite PET study approach. *Alzheimer's Res Ther*. 2021;13:1–10.
  35. Vandenberghe R, Van Laere K, Ivanoiu A, Salmon E, Bastin C, Triau E, Hasselbalch S, Law I, Andersen A, Korner A. 18F-flutemetamol amyloid imaging in Alzheimer disease and mild cognitive impairment: a phase 2 trial. *Ann Neurol*. 2010;68:319–29.
  36. Ribaldi F, Chicherio C, Altomare D, Martins M, Tomczyk S, Jelescu I, Maturana E, Scheffler M, Haller S, Lövsblad K. Brain connectivity and metacognition in persons with subjective cognitive decline (COSCODE): rationale and study design. *Alzheimer's Res Ther*. 2021;13:1–8.
  37. Albert MS, DeKosky ST, Dickson D, Dubois B, Feldman HH, Fox NC, Gamst A, Holtzman DM, Jagust WJ, Petersen RC. The diagnosis of mild cognitive impairment due to Alzheimer's disease: recommendations from the National Institute on Aging-Alzheimer's Association workgroups on diagnostic guidelines for Alzheimer's disease. *Alzheimer's Dement*. 2011;7:270–9.
  38. McKhann GM, Knopman DS, Chertkow H, Hyman BT, Jack CR Jr, Kawas CH, Klunk WE, Koroshetz WJ, Manly JJ, Mayeux R. The diagnosis of dementia due to Alzheimer's disease: Recommendations from the National Institute on Aging-Alzheimer's Association workgroups on diagnostic guidelines for Alzheimer's disease. *Alzheimer's Dement*. 2011;7:263–9.
  39. Saykin AJ, Shen L, Foroud TM, Potkin SG, Swaminathan S, Kim S, Risacher SL, Nho K, Huentelman MJ, Craig DW. Alzheimer's disease neuroimaging initiative biomarkers as quantitative phenotypes: genetics core aims, progress, and plans. *Alzheimer's Dement*. 2010;6:265–73.
  40. Jagust WJ, Landau SM, Koeppe RA, Reiman EM, Chen K, Mathis CA, Price JC, Foster NL, Wang AY. The Alzheimer's disease neuroimaging initiative 2 PET core: 2015. *Alzheimer's Dement*. 2015;11:757–71.
  41. Leuzy A, Pascoal TA, Strandberg O, Insel P, Smith R, Mattsson-Carlsson N, Benedet AL, Cho H, Lyoo CH, La Joie R. A multicenter comparison of [18F] flortaucipir, [18F] RO948, and [18F] MK6240 tau PET tracers to detect a common target ROI for differential diagnosis. *Eur J Nucl Med Mol Imaging*. 2021;48:2295–305.
  42. Lowe VJ, Curran G, Fang P, Liesinger AM, Josephs KA, Parisi JE, Kantarci K, Boeve BF, Pandey MK, Bruinsma T. An autoradiographic evaluation of AV-1451 Tau PET in dementia. *Acta Neuropathol Commun*. 2016;4:1–19.
  43. Biernacki C, Celeux G, Govaert G. Assessing a mixture model for clustering with the integrated completed likelihood. *IEEE Trans Pattern Anal Mach Intell*. 2000;22:719–25.

44. Schöll M, Lockhart SN, Schonhaut DR, O'Neil JP, Janabi M, Ossenkoppele R, Baker SL, Vogel JW, Faria J, Schwimmer HD. PET imaging of tau deposition in the aging human brain. *Neuron*. 2016;89:971–82.
45. Lowe VJ, Wiste HJ, Senjem ML, Weigand SD, Therneau TM, Boeve BF, Josephs KA, Fang P, Pandey MK, Murray ME. Widespread brain tau and its association with ageing. *Braak Stage Alzheimer's Dement Brain*. 2018;141:271–87.
46. Ossenkoppele R, Leuzy A, Cho H, Sudre CH, Strandberg O, Smith R, Palmqvist S, Mattsson-Carlsson N, Olsson T, Jögi J, Stormrud E, Ryu YH, Choi JY, Alzheimer's Disease Neuroimaging Initiative, PREVENT-AD research group, Boxer AL, Gorno-Tempini ML, Miller BL, Soleimani-Meigooni D, Iaccarino L, et al. The impact of demographic, clinical, genetic, and imaging variables on tau PET status. *Eur J Nucl Med Mol Imaging*. 2021;48:2245–58.
47. Busche MA, Hyman BT. Synergy between amyloid- $\beta$  and tau in Alzheimer's disease. *Nat Neurosci*. 2020;23:1183–93.
48. Cho H, Choi JY, Hwang MS, Kim YJ, Lee HM, Lee HS, Lee JH, Ryu YH, Lee MS, Lyoo CH. In vivo cortical spreading pattern of tau and amyloid in the Alzheimer disease spectrum. *Ann Neurol*. 2016;80:247–58.
49. Altomare D, Caprioglio C, Assal F, Allali G, Mendes A, Ribaldi F, Ceyzeriat K, Martins M, Tomczyk S, Stampacchia S. Diagnostic value of amyloid-PET and tau-PET: a head-to-head comparison. *Eur J Nuclear Med Mol Imaging*. 2021;48:2200–11.
50. Cicchetti DV. Guidelines, criteria, and rules of thumb for evaluating normed and standardized assessment instruments in psychology. *Psychol Assess*. 1994;6:284.
51. Soleimani-Meigooni DN, Iaccarino L, La Joie R, Baker S, Bourakova V, Boxer AL, Edwards L, Eser R, Gorno-Tempini M, Jagust WJ. 18F-flortaucipir PET to autopsy comparisons in Alzheimer's disease and other neurodegenerative diseases. *Brain*. 2020;143:3477–94.
52. Jack CR Jr, Knopman DS, Jagust WJ, Petersen RC, Weiner MW, Aisen PS, Shaw LM, Vemuri P, Wiste HJ, Weigand SD, Lesnick TG, Pankratz VS, Donohue MC, Trojanowski JQ. Tracking pathophysiological processes in Alzheimer's disease: an updated hypothetical model of dynamic biomarkers. *Lancet Neurol*. 2013;12:207–16.
53. Schöll M, Maass A, Mattsson N, Ashton NJ, Blennow K, Zetterberg H, Jagust W. Biomarkers for tau pathology. *Mol Cell Neurosci*. 2019;97:18–33.
54. Alexopoulos P, Roesler J, Thierjung N, Werle L, Buck D, Yakushev I, Gleixner L, Kagerbauer S, Ortner M, Grimmer T. Mapping CSF biomarker profiles onto NIA-AA guidelines for Alzheimer's disease. *Eur Arch Psychiatry Clin Neurosci*. 2016;266:587–97.
55. Jack CR, Knopman DS, Chételat G, Dickson D, Fagan AM, Frisoni GB, Jagust W, Mormino EC, Petersen RC, Sperling RA. Suspected non-Alzheimer disease pathophysiology—concept and controversy. *Nat Rev Neurol*. 2016;12:117–24.
56. Crary JF, Trojanowski JQ, Schneider JA, Abisambra JF, Abner EL, Alafuzoff I, Arnold SE, Attems J, Beach TG, Bigio EH, Cairns NJ, Dickson DW, Gearing M, Grinberg LT, Hof PR, Hyman BT, Jellinger KA, Jicha GA, Kovacs GG, et al. Primary age-related tauopathy (PART): a common pathology associated with human aging. *Acta Neuropathol*. 2014;128:755–66.
57. Clark CM, Schneider JA, Bedell BJ, Beach TG, Bilker WB, Mintun MA, Pontecorvo MJ, Hefti F, Carpenter AP, Flitter ML. Use of florbetapir-PET for imaging  $\beta$ -amyloid pathology. *JAMA*. 2011;305:275–83.
58. Reimand J, Boon BD, Collij LE, Teunissen CE, Rozemuller AJ, van Berckel BN, Scheltens P, Ossenkoppele R, Bouwman F. Amyloid- $\beta$  PET and CSF in an autopsy-confirmed cohort. *Ann Clin Transl Neurol*. 2020;7:2150–60.

**Publisher's note** Springer Nature remains neutral with regard to jurisdictional claims in published maps and institutional affiliations.